



*Dedicated to Prof. Ion Grosu
on the occasion of his 70th anniversary*

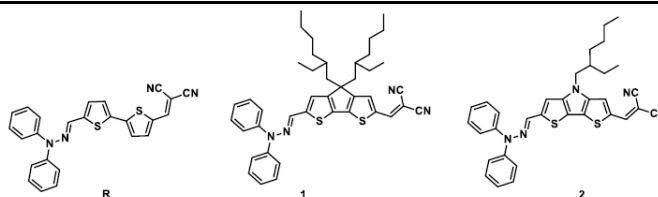
EFFECT OF π -SPACER RIGIDIFICATION ON THE OPTOELECTRONIC PROPERTIES AND PHOTOVOLTAIC PERFORMANCE OF SMALL D- π -A MOLECULES**

Andreea Petronela CRIȘAN, Elena BOGDAN, Lidia CĂTA, Niculina D. HĂDADE and Anamaria TERC*

“Babeș-Bolyai” University, Faculty of Chemistry and Chemical Engineering, Supramolecular Organic and Organometallic Chemistry Centre, 11 Arany Janos, RO-400028 Cluj-Napoca, Roumania

Received February 24, 2025

This study investigates the impact of π -spacer rigidification on the optoelectronic and photovoltaic properties of small donor- π -acceptor (D- π -A) hydrazone-based molecules. Two new derivatives incorporating cyclopentadithiophene (CPDT) and dithienopyrrole (DTP) as rigid π -spacers were synthesized and characterized. Optical and electrochemical analyses reveal a red-shifted absorption profile and altered HOMO-LUMO energy levels compared to the reference molecule containing a non-fused bithiophene spacer. Despite enhanced light absorption, bilayer heterojunction solar cells based on these compounds exhibit lower power conversion efficiencies most probably because of the reduced short-circuit current density and fill factor. These results underscore the complex interplay between molecular design, charge transport, and device performance, providing valuable insights for the development of high-efficiency organic photovoltaic materials.



INTRODUCTION

Organic Solar Cells (OSCs) have emerged lately as one of the most promising low-cost, renewable energy technology and a sustainable alternative to the established silicon-based solar cell technology due to their advantageous solution processability, light-weightness, and transparency.^{1,2}

Extensive research was conducted in the field toward developing more efficient materials alongside optimization of the devices.^{3–7} The power conversion efficiencies (PCEs) of OSCs have recently surpassed the 20% threshold that makes these devices highly attractive for commercialization.^{8–10}

In one of the most efficient OSC architectures, the photo-active layer of a typical OSC with a bulk-heterojunction (BHJ) structure consists of a blend of organic p-type donor material (D) and n-type acceptor material (A). For the acceptor, fullerene and its derivatives were extensively used, while later developed non-fullerene polymers and small molecules showed improved results.^{11–15} Polymeric donors were typically used in early OSCs, but now a plethora of small molecule donors (SMDs) can also be used.^{6,7,15–20} Key requirements in achieving high-performing OSCs devices are the compatibility between donor and acceptor materials, and

* Corresponding author: Anamaria.terec@ubbcluj.ro

** Supplementary information on <https://www.icf.ro/rrch/> or <https://revroum.lew.ro>

controlling the morphology of the active layer.^{21–25} Small molecules have a well-defined molecular structure that brings competitive advantages compared to their polymeric counterparts such as more control over the band structure, ease of purification, batch-to-batch homogeneity, etc.

However, the photovoltaic characteristics (power conversion efficiency *PCE*, short-current density J_{sc} , and open circuit voltage V_{oc}) of small molecule-based OSCs are still inferior to those of polymer-based ones. The design of efficient SDMs aims at narrow optical band gaps (small difference between the energy level of the highest occupied molecular orbital (HOMO) and that of the lowest unoccupied molecular orbital (LUMO)) and appropriate HOMO and LUMO levels, broad absorption maxima and high charge mobility. Integrating a D– π –bridge–A unit in the structure is a commonly reported method to generate narrow band gap materials. Fine-tuning of the properties is achieved by varying the electron-donating and electron-withdrawing effect of the participating units and substituents resulting in materials with efficient charge transfer that delivers large extinction coefficients and broad absorption bands.^{26–28}

One of the most popular electron-rich motifs in conjugated small molecules and polymeric materials is thiophene. However, free rotation around the single bonds in conjugated oligo-thiophenes decreases the coplanarity of the adjacent thiophene units, resulting in a drop in the photovoltaic performance. The π -system could be rigidified into a coplanar conformation by ring fusion. Thus, fused tricyclic systems, such as cyclopenta[2,1-*b*:3,4-*b'*]dithiophene (CPDT) and dithieno[3,2-*b*:2',3'-*d*]pyrrole (DTP), provide better conjugation in the bridge and the rigidification of the backbone resulted, in most cases, in enhanced light absorption properties and molecular organization leading to significant improvements of the electric properties.^{29–31} Both CPDT and DTP building blocks

are widely used in organic photovoltaics^{13,18,20,27,29,31–37} due to their good environmental stability and suitable energy levels and bandgaps.

On the other hand, recent efforts were concentrated on diminishing the cost of the active materials by decreasing the synthetic complexity and the environmental impact by reducing the number of synthetic steps involving metal-catalyzed cross-coupling reactions and replacing them with benign and efficient condensation reactions. One approach makes use of arylhydrazone that can be easily obtained from carbonyl derivatives by condensation, maintains the extended conjugated system, and have electron-donating ability ensuring narrow optical gaps while being thermally stable.³⁸ Hydrazones have been largely employed in organic photovoltaics, mainly in dye sensitized solar cells (DSSCs)^{34,39–43}, perovskite solar cells (PSCs)^{44–46} and donors in OSCs.^{47–50}

In our previous work, we demonstrated that linking an *N,N'*-diphenylhydrazone donor unit to a dicyanovinyl acceptor *via* non-fused thiophene spacers (**R** in Chart 1) positively influences the optoelectronic properties and device performance.⁴⁷ This study presents two newly designed donor– π –acceptor (D– π –A) small molecules, **1** and **2** (Chart 1), that incorporate rigid fused heterocycles — CPDT and DTP, respectively, decorated with branched alkyl moieties to favor solubilization — as π -spacers, along with hydrazone-based electron-donating groups. This molecular design, which has seen limited exploration in previous studies, employs a push–pull framework, where the *N,N'*-diphenylhydrazone acts as the electron-donating "push" component and the dicyanovinyl group serves as the electron-accepting "pull" moiety. The study aims to investigate the impact of π -spacer rigidification on the optoelectronic and photovoltaic behavior of small-molecule D–A systems **1** and **2** in comparison to the non-fused **R**.

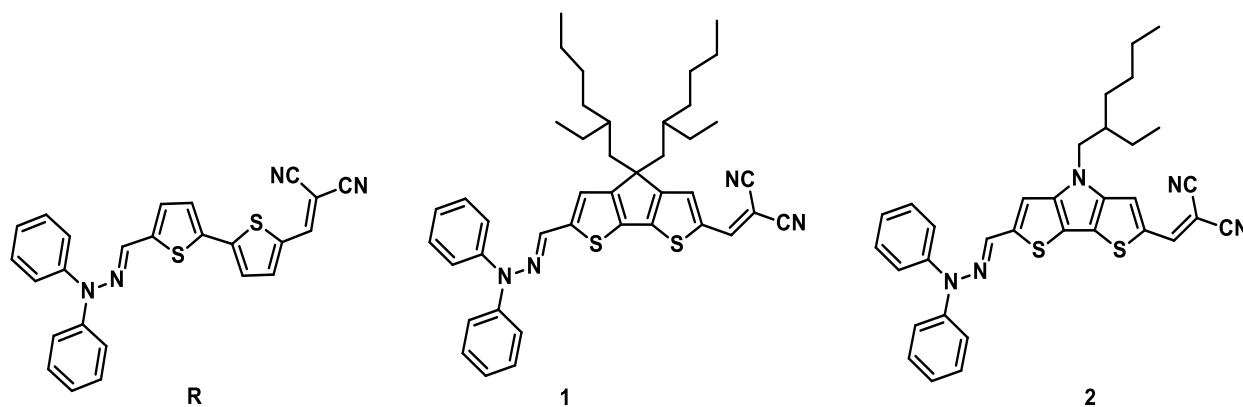
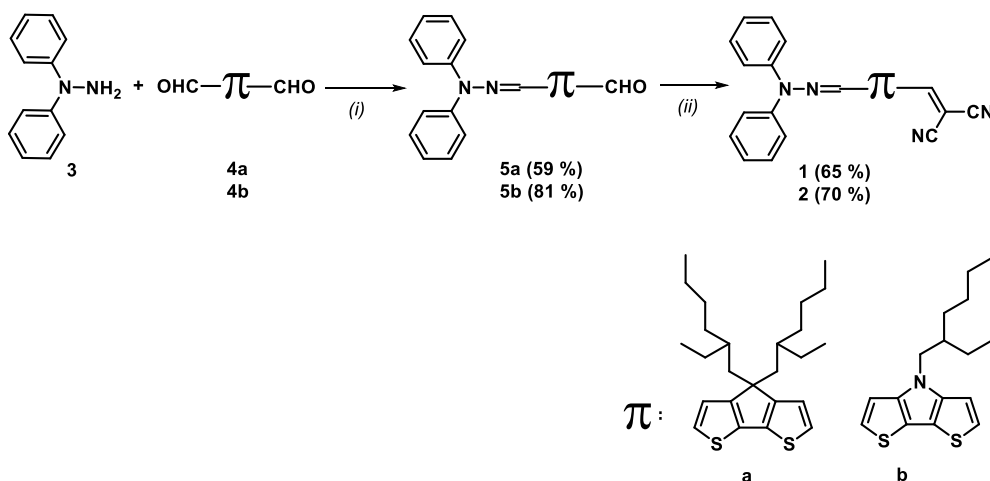


Chart 1 – Structure of investigated compounds.

RESULTS AND DISCUSSION

Synthesis

The synthesis of the target compounds is outlined in Scheme 1. The corresponding dicarboxaldehydes **4a** and **4b** were prepared following a previously published method.¹⁸ Derivatives **1** and **2** were synthesized following a



Scheme 1 – Synthesis of the D- π -A target compounds **1**, **2**. (i) AcONa, MeOH/THF; (ii) CH₂(CN)₂, Et₃N, CHCl₃.

Optical properties

The absorption properties of compounds **1** and **2** were studied in both dichloromethane solution and thin films spin-cast on glass from a chloroform solution, with reference compound **R** used for comparison. Figure 1 shows the UV-vis absorption spectra, and the relevant data are provided in Table 1. All compounds exhibit a low wavelength absorption band in the near-UV region (300–400 nm), attributed to π - π^* electron transitions, followed by a stronger band in the visible region (500–600 nm), which corresponds to an internal charge transfer (ICT) from the *N,N'*-diphenylhydrazone donor unit to the dicyanovinyl acceptor group.^{47,51} As indicated in Table 1 and the UV-vis spectra of compounds **1** and **2** (Fig. 1), the introduction of a rigidified π -spacer with three fused rings (dithienocyclopentadiene and dithienopyrrole) leads to a bathochromic shift of the absorption maximum (λ_{max}), from 533 nm for reference compound **R** (which contains a non-fused bithiophene) to 563 nm for compound **1** and 553 nm for compound **2**. Notably, compound **2** exhibits an absorption maximum that is blue-shifted by 10 nm relative to compound **1**. This hypsochromic shift

previously established stepwise protocol.⁴⁷ Subsequently, condensation of *N,N'*-diphenylhydrazine **3** with the corresponding dicarboxaldehyde derivatives **4** afforded hydrazones **5** in fair yields. Finally, the target compounds **1** and **2** were obtained *via* Knoevenagel condensation of aldehydes **5** with malonodinitrile in chloroform, using triethylamine as a base, with yields of 65% and 70%, respectively.

observed for the DTP spacer, compared to the CPDT counterpart, suggests that the nitrogen bridge reduces the efficiency of the charge transfer process, thereby supporting the intramolecular charge transfer (ICT) nature of the main electronic transition.⁵¹ This behavior is consistent with trends previously reported for other D- π -A systems incorporating similar π -bridges.^{52,53} In the case of thin films, all compounds show a red-shift of λ_{max} and the long-wavelength absorption band, which can be attributed to intermolecular interactions in the solid state. The optical band gap ($E_{\text{opt}}^{\text{g}}$), determined from the onset of the long-wavelength absorption band in the films, is approximately 1.85 eV, indicating that rigidifying the spacer does not significantly impact the optical band gap. This can be attributed to their comparable electronic architectures in terms of donor-acceptor framework and π -conjugated system extent. Furthermore, in similar donor-acceptor (D-A) systems reported in the literature,⁵² DFT calculations have shown that HOMO-LUMO transitions typically involve orbitals of the same character, with the HOMO localized on the donor and the LUMO on the acceptor units, resulting in closely related energy gaps.

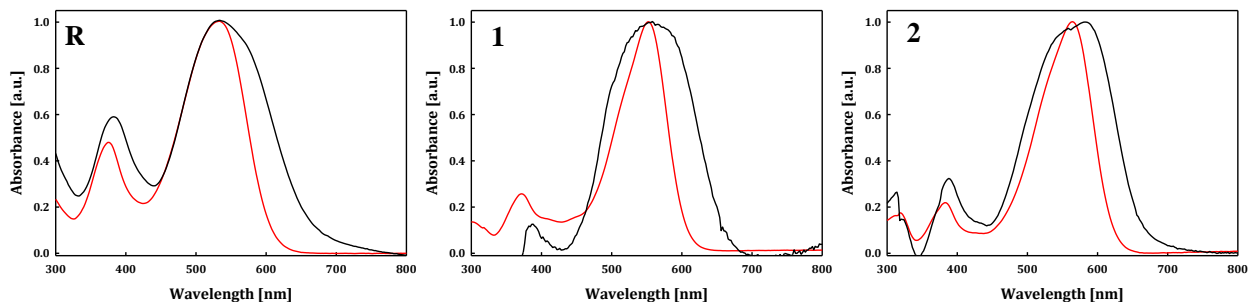


Fig. 1 – UV-Vis absorption spectra of reference and target compounds in solution (red lines) and as spin-cast films (black lines).

Table 1

Optical and electrochemical data for reference (**R**) and target compounds (**1**, **2**): ^s: CH₂Cl₂ solutions; ^f: thin films on glass; ^a: estimated from the long-wavelength absorption onset of thin films; ^b: estimated from the onset of the oxidation and reduction processes; ^c: band gap calculated from the difference between HOMO-LUMO levels

Cmpd	I_{\max}^s [nm]	I_{\max}^f [nm]	E_g^{opt} [eV] ^a	E_{pa} [V]	E_{pc} [V]	E_{HOMO} [eV] ^b	E_{LUMO} [eV] ^b	E_g [eV] ^c
R ^[d]	533	542	1.85	1.02	-1.02	-5.58	-3.81	1.77
1	563	583	1.86	0.90	-1.13	-5.46	-3.66	1.80
2	553	560	1.86	0.93	-1.15	-5.48	-3.65	1.83

[d] From Ref.⁴⁷

Electrochemical properties

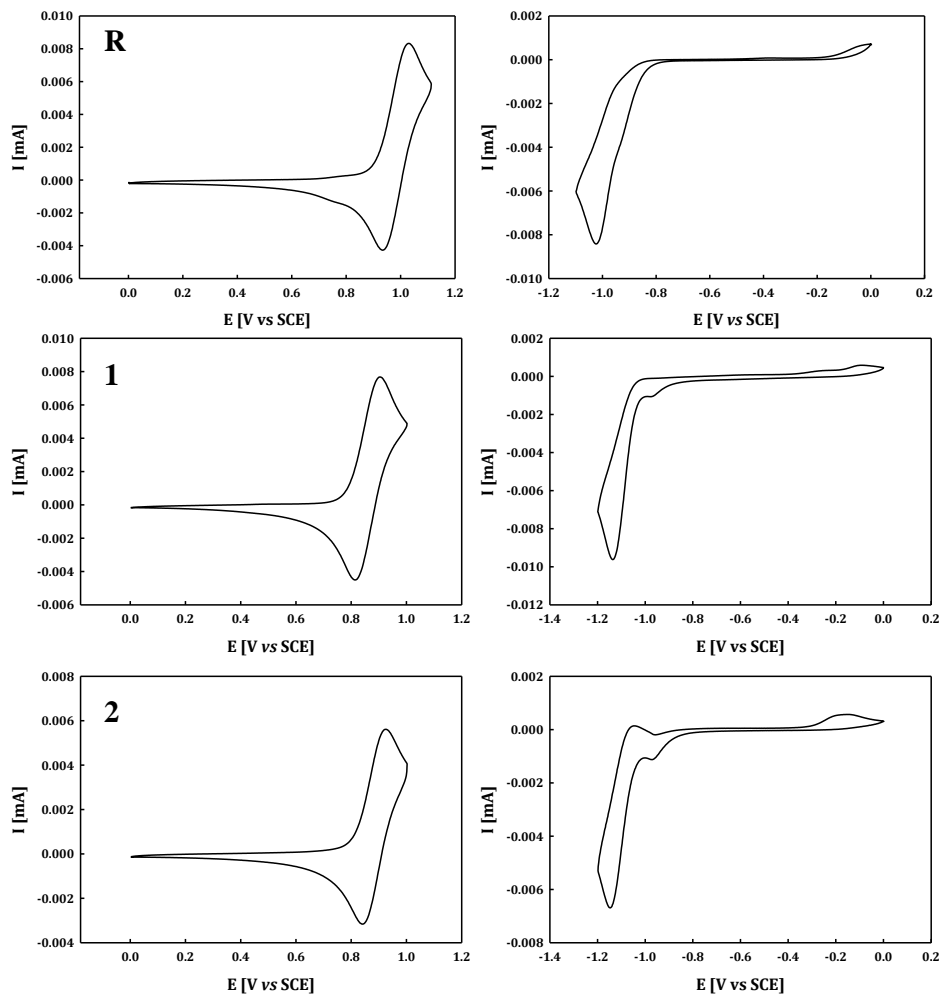


Fig. 2 – Cyclic voltammograms corresponding to the oxidation (left) and reduction (right) of compounds **R**, **1** and **2** in 0.10 M Bu₄NPF₆/CH₂Cl₂, Pt electrodes, scan rate 100mV s⁻¹.

The electrochemical properties of the compounds were investigated using cyclic voltammetry (CV) in dichloromethane, with 0.1M tetrabutylammonium hexafluorophosphate as electrolyte. Figure 2 presents the CV recorded at a scan rate of 100 mV s⁻¹. The CV curves of all three compounds (Fig. 2) show a reversible oxidation wave, indicating the formation of stable radical cations in all cases.

As expected from the UV-vis absorption data, the anodic peak potentials (E_{pa}) decrease from 1.02 V for the reference compound **R** to 0.90 V for compound **1** and to 0.93 V for **2**, respectively (Table 1), highlighting a higher electronic delocalization in **1** and **2** vs. **R**. Compounds **1** and **2** exhibit reversible oxidation waves comparable to those of the reference compound **R**, but with lower onset potentials, suggesting that oxidation occurs more readily, probably due to the increased molecular planarity and rigidity introduced by the CPDT and DTP spacers. In the negative potential region, all compounds exhibit an irreversible reduction wave, with cathodic peak potentials (E_{pc}) shifting from -1.02 V for compound **R** to -1.13 V for compound **1** and -1.15 V for compound **2** (Table 1). The frontier orbital energy levels, estimated from the onset of the oxidation and reduction potentials, confirm that the LUMO levels of all compounds are suitable for photo-induced electron injection into the LUMO of C₆₀.

Photovoltaic properties

This work aims at investigating the impact of subtle structural modifications rather than developing high-performance devices. Therefore, basic planar heterojunction (PHJ) cells are more suitable for analysing structure-property relationships. Consequently, due to their similar optoelectronic properties, the potential of target compounds as donor materials for heterojunction solar cells has been assessed using bilayer PHJ cells with a 0.28 cm² active area, where vacuum-deposited C₆₀ serves as the electron acceptor. PHJ cells were fabricated by spin-coating active films from a chloroform solution on an ITO electrode pre-coated with 40 nm PEDOT:PSS. The substrates were then placed in a vacuum chamber, where a 30 nm thick C₆₀ fullerene acceptor layer was deposited *via* thermal evaporation under a pressure of 4 × 10⁻⁶ mbar and the devices were completed by deposition of a 100 nm layer of aluminium. Each ITO substrate contains two circular cells and each batch typically involves 6–8 cells. After fabrication, the cells underwent a 10-minute thermal treatment at temperatures ranging from 85 to 160°C. Figure 3 shows the current density vs voltage curves for the cells based on compounds **R**, **1**, **2** and the corresponding photovoltaic parameters are listed in Table 2, with the best results highlighted in bold.

Table 2

Photovoltaic Characteristics of **R**, **1**, and **2** using C₆₀ in bilayer solar cells under AM 1.5 simulated solar light conditions with an incident power light of 90 mW cm⁻²

Cmpd	Annealing Temp (°C)	J _{sc} (mA/cm ²)	V _{oc} (V)	FF (%)	PCE (%)
R	ambient	2.48	0.71	37.6	0.75
	average	2.44	0.70	36.8	0.73
	100	5.29	0.78	40.5	1.94
	average	5.40	0.78	39.9	1.93
	120	7.14	0.76	41.9	2.55
	average	7.32	0.74	39.5	2.41
	130	7.84	0.65	39.5	2.26
average	7.91	0.66	37.0	2.19	
1	ambient	1.54	0.66	20.3	0.23
	average	1.22	0.64	20.4	0.20
	80	2.45	0.77	21.3	0.47
	average	2.12	0.67	21.3	0.34
	85	3.11	0.64	19.6	0.56
average	2.92	0.67	21.8	0.47	
2	ambient	2.01	0.42	22.9	0.22
	average	1.84	0.33	24.1	0.19
	120	3.78	0.55	28.2	0.66
	average	3.78	0.52	28.5	0.62
	130	5.88	0.53	28.3	1.00
average	5.47	0.52	29.0	0.92	

A preliminary analysis of the current density vs. voltage curves (Figure 3) of derivatives **1** and **2** clearly demonstrates that the introduction of a rigidified spacer between the donor and acceptor units has a significant impact on cell performance. In particular, the power conversion efficiency, *PCE*, decreases from 2.55% for the reference compound **R** to 0.56% for compound **1** and 1.00% for compound **2**. This reduction is mainly due to a decline of the short-circuit current density (J_{sc}) from 7.14 mA/cm² to 3.11 mA/cm² and 5.88 mA/cm², respectively, along with a decrease of the open circuit voltage (V_{oc}) and fill factor (FF). The

reduced short-circuit current density (J_{sc}) observed for compounds **1** and **2** relative to the reference compound **R** can be attributed to changes in molecular packing and charge transport properties. Importantly, a 10-minute annealing at various temperatures was found to enhance cell performance in all three cases. Moreover, a comparison between derivatives **1** and **2** reveals that the use of a DTP spacer instead of a CPDT one leads to improved photovoltaic characteristics, suggesting that charge recombination between electrons and holes is significantly suppressed with the DTP unit.

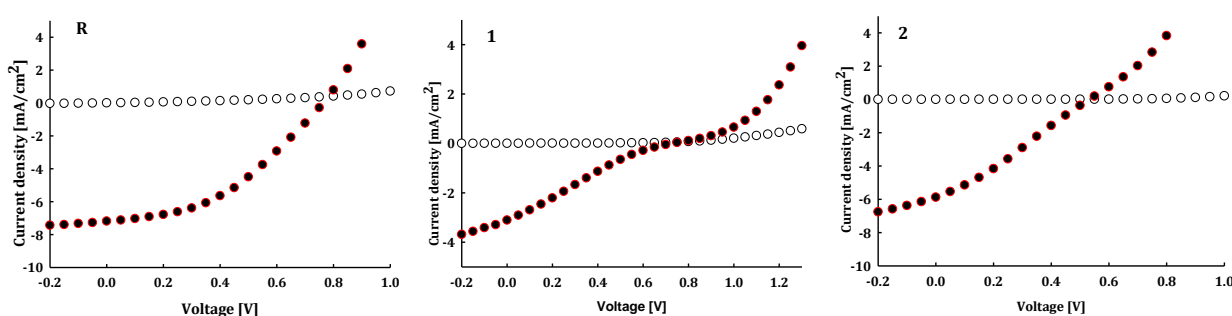


Fig. 3 – Current-density vs voltage curves for bi-layer photovoltaic cells ITO/PEDOT:PSS/D/C₆₀/Al based on spin-cast donors **R**, **1** and **2**. Empty circles: in the dark; black/red circles: under AM 1.5 simulated solar light with an incident power light of 90 mW cm⁻².

To further support these observations, the external quantum efficiency (EQE) spectra of the obtained cells were recorded under monochromatic irradiation and are presented in Figure 4. All devices exhibit a sharp initial peak at 370–380 nm, attributed to the contribution of C₆₀ to the photocurrent. The EQE measurements of these PHJ cells reveal a first band at 430 nm, followed by a broad response spanning 500–700 nm, with a maximum value of approximately 40% at 522 nm for the reference compound **R**, around 13% at 595 nm for compound **1**, and about 33% at 530 nm for compound **2**. The EQE response of compound **1** closely mirrors that of compound **2**, with the main

difference being the higher intensity observed for donor **2**, in agreement with the J_{sc} values. The reduced EQE observed for compound **1** is likely attributed to its lower short-circuit current density (J_{sc}) and potentially a less efficient charge separation. Additionally, the presence of two bulky ethylhexyl side chains in compound **1** may disrupt molecular packing within the active layer, hindering exciton diffusion and charge extraction. The extended photo-response from 400 nm to 700 nm aligns with the absorption spectra of the compounds in the solid state, indicating that the donor layer plays a dominant role in the photocurrent generation.

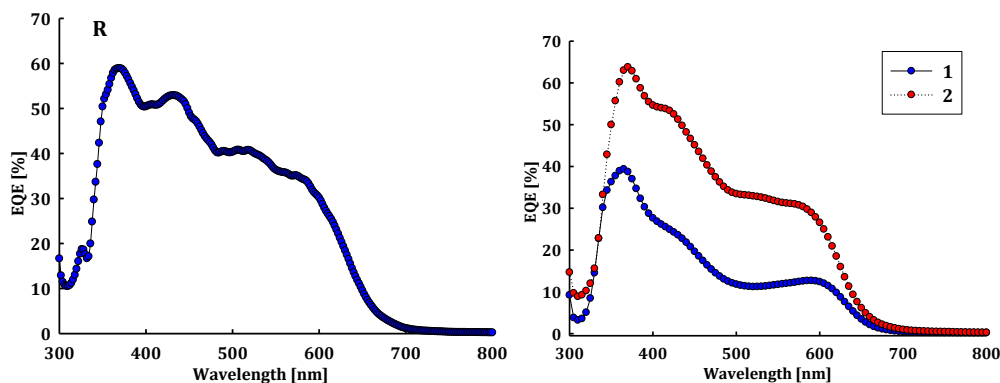


Fig. 4 – Spectra of external quantum efficiency of bi-layer cells based on donors **R**, **1** and **2** under monochromatic irradiation.

EXPERIMENTAL

General

All commercial-grade reagents and chemicals were used without further purification. Solvents were dried and distilled under argon using standard procedures before use. Column chromatography purifications were performed on Merck silica gel Si₆₀ (40–63 μm).

NMR spectra were acquired using a Bruker AVANCE III 300 spectrometer (¹H at 300 MHz, ¹³C at 75 MHz). Chemical shifts are reported in ppm relative to TMS as an internal reference, with coupling constants (*J*) given in Hz. UV-Vis spectra were measured with a Perkin Elmer Lambda 19 or 950 spectrometer.

Melting points were determined using a Reichert-Jung Thermovar hot-stage microscope apparatus and are uncorrected. MALDI-TOF mass spectra were recorded on a BIFLEX III Bruker Daltonics spectrometer with dithranol as the matrix.

Cyclic voltammetry experiments were conducted in dichloromethane solutions (HPLC grade, purchased from SDS). Tetrabutylammonium hexafluorophosphate (0.10 M) was used as a supporting electrolyte (purchased from Across, used without purification). Prior to measurements, solutions were deaerated by nitrogen bubbling. The experiments were performed in a one-compartment electrochemical cell equipped with platinum electrodes and a saturated calomel reference electrode (SCE), using a Biologic SP-150 potentiostat with positive feedback compensation.

Synthesis

(*E*)-6-((2,2-diphenylhydrazono)methyl)-4,4-bis(2-ethylhexyl)-4H-cyclopenta[1,2-*b*:5,4-*b'*]dithiophene-2-carbaldehyde (5a): A solution of *N,N'*-diphenylhydrazine hydrochloride (**3**) (14 mg, 0.065 mmol) and sodium acetate (21 mg, 0.26 mmol) in 4 mL of dry methanol was added dropwise at room temperature under an argon atmosphere to a solution of 4,4-bis(2-ethylhexyl)-4H-cyclopenta[1,2-*b*:5,4-*b'*]dithiophene-2,6-dicarbaldehyde (**4a**) (60 mg, 0.13 mmol) in 30 mL of anhydrous THF. The reaction mixture was then heated at 40°C under inert conditions for 20 hours. After cooling to room temperature, water and methylene chloride

were added. The aqueous phase was extracted twice with dichloromethane, and the combined organic layers were washed with brine and dried over MgSO₄. Following solvent removal, the crude product was purified by silica gel column chromatography using a pentane/diethyl ether (8:1) mixture as the eluent, affording a yellow-orange solid (24 mg, 59 % yield, Mp. 127–129°C). ¹H NMR (CDCl₃, 300 MHz), δ (ppm): 9.81 (s, 1H, CHO), 7.52 (s, 1H, N=CH), 7.47–7.42 (overlapped peaks, 4H, H_{ar}), 7.25–7.19 (overlapped peaks, 7H, H_{ar} and CH (CPDT)), 6.78 (s, 1H, CH (CPDT)), 1.89–1.81 (overlapped peaks, 4H, CH₂ (alkyl)), 0.96–0.85 (overlapped peaks, 18H, CH and CH₂ (alkyl)), 0.75 (m, 6H, CH₃ (alkyl)), 0.59 (m, 6H, CH₃ (alkyl)). ¹³C NMR (CDCl₃, 75 MHz), δ (ppm): 181.7, 149.9, 149.2, 144.7, 143.1, 137.9, 135.8, 135.1, 130.0, 129.5, 126.5, 125.1, 122.6, 114.8, 54.0, 43.3, 35.3, 34.2, 28.6, 27.5, 22.9, 14.2, 10.7. HRMS (MALDI-TOF): calcd. for C₃₉H₄₈N₂OS₂ [M]⁺: 624.3208; found: 624.3195.

(*E*)-6-((2,2-diphenylhydrazono)methyl)-4-(2-ethylhexyl)-4H-dithieno[3,2-*b*:2',3'-*d*]pyrrole-2-carbaldehyde (5b): A solution of *N,N'*-diphenylhydrazine hydrochloride (**3**) (32 mg, 0.14 mmol) and sodium acetate (76 mg, 0.92 mmol) in 6 mL of dry methanol was gradually added to a solution of 4-(2-ethylhexyl)-4H-dithieno[3,2-*b*:2',3'-*d*]pyrrole-2,6-dicarbaldehyde (**4b**) (100 mg, 0.29 mmol) in 40 mL of anhydrous THF at room temperature. The reaction mixture was then heated to 50°C under an argon atmosphere for 20 hours. After cooling to room temperature, dichloromethane was added, and the organic phase was washed with water and dried over MgSO₄. Following solvent removal, the crude product was purified by silica gel chromatography using a diethyl ether/pentane (3:2) mixture as the eluent, yielding an orange-brown solid (60 mg, 81% yield, Mp. 153–155°C). ¹H NMR (CDCl₃, 300 MHz), δ (ppm): 9.85 (s, 1H, CHO), 7.55 (s, 1H, N=CH), 7.47–7.42 (overlapped peaks, 4H, H_{ar}), 7.29 (s, 1H, CH (DTP)), 7.25–7.20 (overlapped peaks, 6H, H_{ar}), 6.78 (s, 1H, CH (DTP)), 4.00 (dd, 2H, *J* = 7.2 Hz, *J* = 2.7 Hz, CH₂ (alkyl)), 1.88 (m, 1H, CH (alkyl)), 1.32–1.26 (overlapped peaks, 8H, CH₂ (alkyl)), 0.85–0.90 (overlapped peaks, 6H, CH₃ (alkyl)). ¹³C NMR (CDCl₃, 75 MHz), δ (ppm): 182.9, 149.2, 145.4, 145.1, 145.0, 143.2, 140.3, 130.2, 130.0, 125.1, 123.7, 122.6, 114.6, 109.7, 51.5, 40.5, 30.8, 28.8, 24.1, 23.1, 14.1, 10.8. HRMS (MALDI-TOF): calcd. for C₃₀H₃₁N₃OS₂ [M]⁺: 513.1909; found: 513.1895.

(E)-2-((6-((2,2-diphenylhydrazono)methyl)-4,4-bis(2-ethylhexyl)-4H-cyclopenta[1,2-b:5,4-b']dithio-phen-2-yl)methylene)malononitrile

(1): Malonodinitrile (4 mg, 0.048 mmol) and a drop of triethylamine were added to a solution of **5a** (20 mg, 0.032 mmol) in 6 mL of chloroform. The reaction mixture was stirred at room temperature for two hours, followed by an additional two hours at 50°C. After cooling to room temperature, the solution was diluted with methylene chloride, washed with water and brine, and dried over magnesium sulfate. The solvent was then removed, and the crude product was purified by silica gel column chromatography using pentane/diethyl ether (9:1) mixture as the eluent, yielding a violet solid (15 mg, 70% yield, Mp. 88–89°C). ¹H NMR (CDCl₃, 300 MHz), δ (ppm): 7.67 (s, 1H, CH=C(CN)₂), 7.53 (s, 1H, N=CH), 7.48–7.43 (overlapped peaks, 4H, H_{ar}), 7.25–7.19 (overlapped peaks, 7H, H_{ar} and CH (CPDT)), 6.80 (s, 1H, CH (CPDT)), 1.90–1.82 (m, 4H, CH₂ (alkyl)), 0.96–0.87 (overlapped peaks, 18H, CH₂ and CH (alkyl)), 0.75 (m, 6H, CH₃ (alkyl)), 0.59 (m, 6H, CH₃ (alkyl)). ¹³C NMR (CDCl₃, 75 MHz), δ (ppm): 164.2, 152.0, 149.9, 149.5, 143.0, 135.3, 135.1, 130.1, 129.5, 129.4, 125.3, 122.6, 121.2, 121.0, 115.5, 114.8, 71.7, 54.1, 43.2, 35.4, 34.1, 28.6, 27.4, 22.9, 14.2, 10.7. HRMS (MALDI-TOF): calcd. for C₄₂H₄₈N₄S₂ [M]⁺: 672.3320; found: 672.3300.

(E)-2-((6-((2,2-diphenylhydrazono)methyl)-4-(2-ethylhexyl)-4H-dithieno[3,2-b:2',3'-d]pyrrol-2-yl)methylene)malononitrile

(2): Three drops of triethylamine were added to a solution of compound **5b** (80 mg, 0.16 mmol) and malononitrile (16 mg, 0.25 mmol) in 30 mL of chloroform. The mixture was stirred overnight at room temperature under an argon atmosphere. After solvent removal, the crude product was dissolved in dichloromethane, washed with water and brine, dried over magnesium sulfate, and purified by silica gel column chromatography using a pentane/diethyl ether (4:1) mixture as the eluent, yielding a deep-violet solid (60 mg, 65% yield, Mp. 155–157°C). ¹H NMR (CDCl₃, 300 MHz), δ (ppm): 7.65 (s, 1H, CH=C(CN)₂), 7.58 (s, 1H, N=CH), 7.48–7.43 (overlapped peaks, 4H, H_{ar}), 7.28 (s, 1H, CH (DTP)), 7.25–7.20 (overlapped peaks, 6H, H_{ar}), 6.76 (s, 1H, CH (DTP)), 3.98 (dd, 2H, J = 6.9 Hz, J = 2.1 Hz, CH₂ (alkyl)), 1.83–1.89 (m, 1H, CH (alkyl)), 1.33–1.26 (overlapped peaks, 8H, CH₂ (alkyl)), 0.90–0.83 (overlapped peaks, 6H, CH₃ (alkyl)). ¹³C NMR (CDCl₃, 75 MHz), δ (ppm): 151.3, 150.4, 148.3, 146.0, 143.0, 132.4, 130.1, 129.7, 126.8, 125.4, 122.6, 115.7, 115.0, 114.7,

109.3, 71.4, 51.6, 40.5, 30.8, 28.8, 24.1, 23.1, 14.1, 10.8. HRMS (MALDI-TOF): calcd. for C₃₃H₃₁N₅S₂ [M]⁺: 561.2021; found: 561.2015.

Device fabrication and characterization

Indium-tin oxide (ITO)-coated glass slides (24 mm × 25 mm × 1.1 mm) with a surface resistance of 10 Ω/sq were obtained from Kintec company. Selective etching of the ITO layer was performed using 37% HCl. The electrodes were then sequentially cleaned in an ultrasonic bath with Deconex (VWR International GmbH), distilled water (15.3 MΩ cm⁻¹), acetone, ethanol, and a final rinse with distilled water, each for 10 minutes. After drying in an oven at 100°C, the electrodes were coated with a spun-cast layer of PEDOT:PSS (Clevios P VP AI 4083, HC-Starck), which was filtered through a 0.45 µm membrane immediately before use. Spin-coating was performed at 5000 rpm (ramp time: 10 s, spin time: 60 s), followed by drying at 130°C for 15 minutes.

Various solvents were tested for donor layer deposition, best results were obtained from chloroform (organic material solubility 1 mg/0.1 ml) that provided good quality films. Thin films (~20 nm) of donor materials were spin-cast under ambient conditions from chloroform solutions containing 5 mg/mL of the donor. After deposition, the devices were transferred into an argon-filled glovebox (200B, MBraun) equipped with a vacuum chamber. A 30 nm film of fullerene C₆₀ (99+%, MER Corporation) and a 100 nm thick aluminum electrode were thermally evaporated onto the donor film under a vacuum of 2–4 × 10⁻⁶ mbar using a shadow mask, defining two active cells (6.0 mm diameter, 0.28 cm²) on each ITO electrode.

Current density vs. voltage (J–V) characteristics were recorded in both dark and illuminated conditions using a Keithley 236 source-measure unit and a custom acquisition program. Illumination was provided by an AM1.5 Solar Constant 575 PV simulator (Steuernagel Lichttechnik) equipped with a metal halogen lamp. The incident light intensity (~90 mW cm⁻²) was measured using a broadband power meter (13PEM001, Melles Griot), and devices were illuminated through the ITO electrode side. The reported efficiency values are uncorrected for potential spectral mismatches of the solar simulator.

External quantum efficiency (EQE) measurements were performed using a halogen lamp (Osram) in combination with an Action Spectra Pro 150 monochromator, a Perkin-Elmer 7225 lock-in amplifier, and a S2281 photodiode (Hamamatsu).

CONCLUSIONS

We have successfully synthesized and characterized two new D- π -A molecules, in which a diphenylhydrazone donor unit is connected to a dicyanovinyl acceptor *via* rigidified thiophene-based π -conjugated spacers using a straightforward metal-free approach. Cyclic voltammetry and UV-vis absorption studies demonstrate that the spacer's nature significantly impacts the HOMO-LUMO energy levels and light-harvesting properties. Notably, compounds **1** and **2**, which incorporate three fused rings as π -conjugated spacers, exhibit a red-shifted internal charge transfer band in both solution and thin films, along with a larger electrochemical bandgap compared to the reference compound featuring a non-fused bithiophene spacer. The synthesized molecules were evaluated as *p*-type semiconductors in bi-layer photovoltaic devices using C₆₀ as the *n*-type counterpart. The results revealed that, in our case rigidifying the spacer has a detrimental effect on the photovoltaic performance of CPDT- and DTP-based compounds. Hence, the improved light-harvesting properties of compounds **1** and **2** did not directly translate into enhanced photovoltaic parameters, probably due to inefficient charge separation alongside undesired charge recombination in the photoactive layer. Results obtained with CPDT- and DTP-containing derivatives highlight the challenges in predicting the influence of these building blocks on material organization, electronic properties, and photovoltaic performance. Ongoing efforts aim to enhance the power conversion efficiency of devices, with future studies focusing on leveraging the fused thiophene unit in higher-efficiency D- π -A materials.

Acknowledgements. This work was supported by the Romanian Ministry of Research, Innovation and Digitization, CNCS – UEFISCDI, research projects PN-III-P4-ID-PCE-2020-1812 (ICOFOSC), PN-III-P2-2.1-PED-2019-2601 (REGRENPOS) and 312-COFFEE ERANET within PNCDI IV.

REFERENCES

- Solak, E. K.; Irmak, E. Advances in Organic Photovoltaic Cells: A Comprehensive Review of Materials, Technologies, and Performance. *RSC Adv.* **2023**, *13* (18), 12244–12269. <https://doi.org/10.1039/D3RA01454A>.
- Jain, A.; Kothari, R.; Tyagi, V. V.; Kumar Rajamony, R.; Shakeel Ahmad, M.; Mohan Singh, H.; Raina, S.; Pandey, A. K. Advances in Organic Solar Cells: Materials, Progress, Challenges and Amelioration for Sustainable Future. *Sustain. Energy Technol. Assess.* **2024**, *63*, 103632. <https://doi.org/10.1016/j.seta.2024.103632>.
- Ding, P.; Yang, D.; Yang, S.; Ge, Z. Stability of Organic Solar Cells: Toward Commercial Applications. *Chem. Soc. Rev.* **2024**, *53* (5), 2350–2387. <https://doi.org/10.1039/D3CS00492A>.
- Li, M.; He, F. Organic Solar Cells Developments: What's next? *Energy* **2024**, *2*, 100085. <https://doi.org/10.1016/j.nxener.2023.100085>.
- Liu, Y.; Liu, B.; Ma, C.-Q.; Huang, F.; Feng, G.; Chen, H.; Hou, J.; Yan, L.; Wei, Q.; Luo, Q.; Bao, Q.; Ma, W.; Liu, W.; Li, W.; Wan, X.; Hu, X.; Han, Y.; Li, Y.; Zhou, Y.; Zou, Y.; Chen, Y.; Li, Y.; Chen, Y.; Tang, Z.; Hu, Z.; Zhang, Z.-G.; Bo, Z. Recent Progress in Organic Solar Cells (Part I Material Science). *Sci. China Chem.* **2022**, *65* (2), 224–268. <https://doi.org/10.1007/s11426-021-1180-6>.
- Liu, Y.; Liu, B.; Ma, C.-Q.; Huang, F.; Feng, G.; Chen, H.; Hou, J.; Yan, L.; Wei, Q.; Luo, Q.; Bao, Q.; Ma, W.; Liu, W.; Li, W.; Wan, X.; Hu, X.; Han, Y.; Li, Y.; Zhou, Y.; Zou, Y.; Chen, Y.; Liu, Y.; Meng, L.; Li, Y.; Chen, Y.; Tang, Z.; Hu, Z.; Zhang, Z.-G.; Bo, Z. Recent Progress in Organic Solar Cells (Part II Device Engineering). *Sci. China Chem.* **2022**, *65* (8), 1457–1497. <https://doi.org/10.1007/s11426-022-1256-8>.
- Yi, J.; Zhang, G.; Yu, H.; Yan, H. Advantages, Challenges and Molecular Design of Different Material Types Used in Organic Solar Cells. *Nat. Rev. Mater.* **2023**, *9* (1), 46–62. <https://doi.org/10.1038/s41578-023-00618-1>.
- Zhu, L.; Zhang, M.; Zhou, G.; Wang, Z.; Zhong, W.; Zhuang, J.; Zhou, Z.; Gao, X.; Kan, L.; Hao, B.; Han, F.; Zeng, R.; Xue, X.; Xu, S.; Jing, H.; Xiao, B.; Zhu, H.; Zhang, Y.; Liu, F. Achieving 20.8% Organic Solar Cells via Additive-Assisted Layer-by-Layer Fabrication with Bulk *p-i-n* Structure and Improved Optical Management. *Joule* **2024**, *8* (11), 3153–3168. <https://doi.org/10.1016/j.joule.2024.08.001>.
- Li, C.; Song, J.; Lai, H.; Zhang, H.; Zhou, R.; Xu, J.; Huang, H.; Liu, L.; Gao, J.; Li, Y.; Jee, M. H.; Zheng, Z.; Liu, S.; Yan, J.; Chen, X.-K.; Tang, Z.; Zhang, C.; Woo, H. Y.; He, F.; Gao, F.; Yan, H.; Sun, Y. Non-Fullerene Acceptors with High Crystallinity and Photoluminescence Quantum Yield Enable >20% Efficiency Organic Solar Cells. *Nat. Mater.* **2025**, 1–11. <https://doi.org/10.1038/s41563-024-02087-5>.
- Mohamed El Amine, B.; Zhou, Y.; Li, H.; Wang, Q.; Xi, J.; Zhao, C. Latest Updates of Single-Junction Organic Solar Cells up to 20% Efficiency. *Energies* **2023**, *16* (9), 3895. <https://doi.org/10.3390/en16093895>.
- Lee, M.; Hwang, E.; Kim, T.; Kwon, T.-H. Advancements in Non-Fullerene Acceptors for Organic Solar Cells: Brief Review of Research Trends. *Bull. Korean Chem. Soc.* **2024**, *45* (8), 664–674. <https://doi.org/10.1002/bkcs.12888>.
- Wadsworth, A.; Moser, M.; Marks, A.; Little, M. S.; Gasparini, N.; Brabec, C. J.; Baran, D.; McCulloch, I. Critical Review of the Molecular Design Progress in Non-Fullerene Electron Acceptors towards Commercially Viable Organic Solar Cells. *Chem. Soc. Rev.* **2019**, *48* (6), 1596–1625. <https://doi.org/10.1039/C7CS00892A>.
- Zhang, J.; Liu, L.; Li, H.; Cao, J.; Cao, Y.; Yang, P.; Xiao, M.; Liu, W. Nonfullerene Acceptors Based on Naphthalene Substituted Thieno[3,2-*b*]Thiophene Core for Efficient Organic Solar Cells. *Russ. J. Gen. Chem.* **2022**, *92* (11), 2354–2362. <https://doi.org/10.1134/S1070363222110202>.
- Zhang, G.; Zhao, J.; Chow, P. C. Y.; Jiang, K.; Zhang, J.; Zhu, Z.; Zhang, J.; Huang, F.; Yan, H. Nonfullerene Acceptor Molecules for Bulk Heterojunction Organic Solar Cells. *Chem. Rev.* **2018**, *118* (7), 3447–3507. <https://doi.org/10.1021/acs.chemrev.7b00535>.

15. Sharma, V. V.; Landep, A.; Lee, S.-Y.; Park, S.-J.; Kim, Y.-H.; Kim, G.-H. Recent Advances in Polymeric and Small Molecule Donor Materials for Y6 Based Organic Solar Cells. *Energy* **2024**, *2*, 100086. <https://doi.org/10.1016/j.nxener.2023.100086>.
16. Terenti, N.; Giurgi, G.-I.; Crişan, A. P.; Anghel, C.; Bogdan, A.; Pop, A.; Stroia, I.; Terec, A.; Szolga, L.; Grosu, I.; Roncali, J. Structure–Properties of Small Donor–Acceptor Molecules for Homojunction Single-Material Organic Solar Cells. *J. Mater. Chem. C* **2022**, *10* (14), 5716–5726. <https://doi.org/10.1039/D2TC00430E>.
17. Diac, A. P.; Szolga, L.; Cabanetos, C.; Bogdan, A.; Terec, A.; Grosu, I.; Roncali, J. C60-Small Arylamine Push-Pull Dyads for Single-Material Organic Solar Cells. *Dyes Pigments* **2019**, *171*, 107748. <https://doi.org/10.1016/j.dyepig.2019.107748>.
18. Yassin, A.; Rousseau, T.; Leriche, P.; Cravino, A.; Roncali, J. Evaluation of Bis-Dicyanovinyl Short-Chain Conjugated Systems as Donor Materials for Organic Solar Cells. *Sol. Energy Mater. Sol. Cells* **2011**, *95* (2), 462–468. <https://doi.org/10.1016/j.solmat.2010.08.032>.
19. Giurgi, G.-I.; Szolga, L.; Kovacs, I.; Bogdan, E.; Hădade, N. D.; Terec, A.; Grosu, I.; Roncali, J. Inverted versus Direct Structure Bulk Heterojunction Organic Solar Cells Involving a Triphenylamine-Based Small Molecular Donor. *Stud. Univ. Babeş-Bolyai Chem.* **2020**, *65* (2), 95–106. <https://doi.org/10.24193/subbchem.2020.2.08>.
20. Busireddy, M. R.; Raju Mantena, V. N.; Chereddy, N. R.; Shanigaram, B.; Kotamarthi, B.; Biswas, S.; Sharma, G. D.; Vaidya, J. R. A Dithieno[3,2-*b*:2',3'-*d*]Pyrrole Based, NIR Absorbing, Solution Processable, Small Molecule Donor for Efficient Bulk Heterojunction Solar Cells. *Phys. Chem. Chem. Phys.* **2016**, *18* (47), 32096–32106. <https://doi.org/10.1039/C6CP06304G>.
21. Li, C.; Zhou, J.; Song, J.; Xu, J.; Zhang, H.; Zhang, X.; Guo, J.; Zhu, L.; Wei, D.; Han, G.; Min, J.; Zhang, Y.; Xie, Z.; Yi, Y.; Yan, H.; Gao, F.; Liu, F.; Sun, Y. Non-Fullerene Acceptors with Branched Side Chains and Improved Molecular Packing to Exceed 18% Efficiency in Organic Solar Cells. *Nat. Energy* **2021**, *6* (6), 605–613. <https://doi.org/10.1038/s41560-021-00820-x>.
22. Chen, Z.; Song, W.; Yu, K.; Ge, J.; Zhang, J.; Xie, L.; Peng, R.; Ge, Z. Small-Molecular Donor Guest Achieves Rigid 18.5% and Flexible 15.9% Efficiency Organic Photovoltaic via Fine-Tuning Microstructure Morphology. *Joule* **2021**, *5* (9), 2395–2407. <https://doi.org/10.1016/j.joule.2021.06.017>.
23. Li, J.; Zhang, C.; Sun, X.; Wang, H.; Hu, H.; Wang, K.; Xiao, M. Small Molecule Donor Third Component Incorporating Thieno[3,2-*b*]Thiophene Unit Enables 19.18% Efficiency Ternary Organic Solar Cells with Improved Operational Stability. *Nano Energy* **2024**, *125*, 109542. <https://doi.org/10.1016/j.nanoen.2024.109542>.
24. Zhang, R.; Chen, H.; Wang, T.; Kobera, L.; He, L.; Huang, Y.; Ding, J.; Zhang, B.; Khasbaatar, A.; Nanayakkara, S.; Zheng, J.; Chen, W.; Diao, Y.; Abbrent, S.; Brus, J.; Coffey, A. H.; Zhu, C.; Liu, H.; Lu, X.; Jiang, Q.; Coropceanu, V.; Brédas, J.-L.; Li, Y.; Li, Y.; Gao, F. Equally High Efficiencies of Organic Solar Cells Processed from Different Solvents Reveal Key Factors for Morphology Control. *Nat. Energy* **2025**, *10* (1), 124–134. <https://doi.org/10.1038/s41560-024-01678-5>.
25. Tegegne, N. A.; Nchinda, L. T.; Krüger, T. P. J. Progress Toward Stable Organic Solar Cells. *Adv. Opt. Mater.* **2025**, *13* (4), 2402257. <https://doi.org/10.1002/adom.202402257>.
26. Scharber, M. C.; Mühlbacher, D.; Koppe, M.; Denk, P.; Waldauf, C.; Heeger, A. J.; Brabec, C. J. Design Rules for Donors in Bulk-Heterojunction Solar Cells—Towards 10 % Energy-Conversion Efficiency. *Adv. Mater.* **2006**, *18* (6), 789–794. <https://doi.org/10.1002/adma.200501717>.
27. Lucas, S.; Kammerer, J.; Pfannmöller, M.; Schröder, R. R.; He, Y.; Li, N.; Brabec, C. J.; Leydecker, T.; Samori, P.; Marszalek, T.; Pisula, W.; Mena-Osteritz, E.; Bäuerle, P. Molecular Donor–Acceptor Dyads for Efficient Single-Material Organic Solar Cells. *Sol. RRL* **2021**, *5* (1), 2000653. <https://doi.org/10.1002/solr.202000653>.
28. Khasbaatar, A.; Xu, Z.; Lee, J.-H.; Campillo-Alvarado, G.; Hwang, C.; Onusaitis, B. N.; Diao, Y. From Solution to Thin Film: Molecular Assembly of π -Conjugated Systems and Impact on (Opto)Electronic Properties. *Chem. Rev.* **2023**, *123* (13), 8395–8487. <https://doi.org/10.1021/acs.chemrev.2c00905>.
29. Gupta, A.; Ali, A.; Gao, M.; Singh, Th. B.; Bilic, A.; Watkins, S. E.; Bach, U.; Evans, R. A. Small Molecules Containing Rigidified Thiophenes and a Cyanopyridone Acceptor Unit for Solution-Processable Bulk-Heterojunction Solar Cells. *Dyes Pigments* **2015**, *119*, 122–132. <https://doi.org/10.1016/j.dyepig.2015.03.028>.
30. Zhou, E.; Hashimoto, K.; Tajima, K. Low Band Gap Polymers for Photovoltaic Device with Photocurrent Response Wavelengths over 1000 nm. *Polymer* **2013**, *54* (24), 6501–6509. <https://doi.org/10.1016/j.polymer.2013.09.058>.
31. Geng, Y.; Tang, A.; Tajima, K.; Zeng, Q.; Zhou, E. Conjugated Materials Containing Dithieno[3,2-*b*:2',3'-*d*]Pyrrole and Its Derivatives for Organic and Hybrid Solar Cell Applications. *J. Mater. Chem. A* **2018**, *7* (1), 64–96. <https://doi.org/10.1039/C8TA09383K>.
32. Liu, K.; Zheng, S. A Computational Investigation of the Effects of Changes of Donor–Acceptor Linker Length and Acceptor on Electronic Spectra of Small-Molecule Single-Component Organic Solar Cells. *Chem. Phys.* **2024**, *579*, 112169. <https://doi.org/10.1016/j.chemphys.2023.112169>.
33. Li, M.; Ni, W.; Feng, H.; Kan, B.; Wan, X.; Zhang, Y.; Yang, X.; Chen, Y. Dithienopyrrole Based Small Molecule with Low Band Gap for Organic Solar Cells. *Chin. J. Chem.* **2015**, *33* (8), 852–858. <https://doi.org/10.1002/cjoc.201500170>.
34. Gupta, A.; Kelson, M. M. A.; Armel, V.; Bilic, A.; Bhosale, S. V. N-Alkyl- and N-Aryl-Dithieno[3,2-*b*:2',3'-*d*]Pyrrole-Containing Organic Dyes for Efficient Dye-Sensitized Solar Cells. *Tetrahedron* **2014**, *70* (12), 2141–2150. <https://doi.org/10.1016/j.tet.2014.02.002>.
35. Zhang, Z.-B.; Xu, J.-W.; Zhang, X.-Y.; Sun, S.-X.; Xing, R. Novel Dithienopyrrole-Based Molecular Donor Materials for Organic Solar Cells. *Funct. Mater. Lett.* **2017**, *10* (06), 1750085. <https://doi.org/10.1142/S1793604717500850>.
36. Zheng, R.; Guo, Q.; Hao, D.; Zhang, C.; Xue, W.; Huang, H.; Li, C.; Ma, W.; Bo, Z. Naphthalene Core-Based Noncovalently Fused-Ring Electron Acceptors: Effects of Linkage Positions on Photovoltaic Performances. *J. Mater. Chem. C* **2019**, *7* (48), 15141–15147. <https://doi.org/10.1039/C9TC05013B>.
37. Shi, Y.; Pan, J.; Zhang, H.; Yang, C.; Zhang, Z.; Deng, D.; Zhang, J.; Lu, K.; Wei, Z. The Substituents on the

- Intermediate Electron-Deficient Groups in Small Molecular Acceptors Result Appropriate Morphologies for Organic Solar Cells. *Org. Electron.* **2021**, *93*, 106133. <https://doi.org/10.1016/j.orgel.2021.106133>.
38. Lygaitis, R.; Getautis, V.; Grazulevicius, J. V. Hole-Transporting Hydrazones. *Chem. Soc. Rev.* **2008**, *37* (4), 770–788. <https://doi.org/10.1039/B702406C>.
39. Al-Sehemi, A. G.; Allami, S. A. S.; Kalam, A. Design and Synthesis of Organic Dyes with Various Donor Groups: Promising Dyes for Dye-Sensitized Solar Cells. *Bull. Mater. Sci.* **2020**, *43* (1), 224. <https://doi.org/10.1007/s12034-020-02198-0>.
40. Erden, I.; Orman, Z.; Kilicarslan, F. A. Effect of Different π -Conjugated Dyes Containing 4,5-Diazafluorenone-9-Hydrazoni on The Performance of Dye-Sensitized Solar Cells. *J. Struct. Chem.* **2018**, *59* (6), 1335–1341. <https://doi.org/10.1134/S0022476618060124>.
41. Al-Sehemi, A. G.; Irfan, A.; Asiri, A. M.; Ammar, Y. A. Molecular Design of New Hydrazone Dyes for Dye-Sensitized Solar Cells: Synthesis, Characterization and DFT Study. *J. Mol. Struct.* **2012**, *1019*, 130–134. <https://doi.org/10.1016/j.molstruc.2012.02.035>.
42. Urnikaite, S.; Daskeviciene, M.; Send, R.; Wonneberger, H.; Sackus, A.; Bruder, I.; Getautis, V. Organic Dyes Containing a Hydrazone Moiety as Auxiliary Donor for Solid-State DSSC Applications. *Dyes Pigments* **2015**, *114*, 175–183. <https://doi.org/10.1016/j.dyepig.2014.11.012>.
43. Urnikaite, S.; Malinauskas, T.; Bruder, I.; Send, R.; Gaidelis, V.; Sens, R.; Getautis, V. Organic Dyes with Hydrazone Moieties: A Study of Correlation between Structure and Performance in the Solid-State Dye-Sensitized Solar Cells. *J. Phys. Chem. C* **2014**, *118* (15), 7832–7843. <https://doi.org/10.1021/jp500527d>.
44. Decavoli, C.; Boldrini, C. L.; Abbotto, A.; Manfredi, N. Economical and Environmentally Friendly Organic Hydrazone Derivatives Characterized by a Heteroaromatic Core as Potential Hole Transporting Materials in Perovskite Solar Cells. *Eur. J. Org. Chem.* **2023**, *26* (26), e202201511. <https://doi.org/10.1002/ejoc.202201511>.
45. Petrus, M. L.; Sirtl, M. T.; Closs, A. C.; Bein, T.; Docampo, P. Hydrazone-Based Hole Transporting Material Prepared *via* Condensation Chemistry as Alternative for Cross-Coupling Chemistry for Perovskite Solar Cells. *Mol. Syst. Des. Eng.* **2018**, *3* (5), 734–740. <https://doi.org/10.1039/C8ME00023A>.
46. Sun, Z.; Gu, N.; Feng, Y.; Song, L.; Du, P.; Jiang, H.; Xiong, J. Hydrazone Dye Passivator for High-Performance and Stable Perovskite Solar Cells. *Dalton Trans.* **2023**, *52* (6), 1702–1710. <https://doi.org/10.1039/D2DT03957E>.
47. Diac, A.; Demeter, D.; Allain, M.; Grosu, I.; Roncali, J. Simple and Versatile Molecular Donors for Organic Photovoltaics Prepared by Metal-Free Synthesis. *Chem. – Eur. J.* **2015**, *21* (4), 1598–1608. <https://doi.org/10.1002/chem.201405425>.
48. Shen, P.; Liu, X.; Jiang, S.; Huang, Y.; Yi, L.; Zhao, B.; Tan, S. Effects of Aromatic π -Conjugated Bridges on Optical and Photovoltaic Properties of *N,N*-Diphenylhydrazone-Based Metal-Free Organic Dyes. *Org. Electron.* **2011**, *12* (12), 1992–2002. <https://doi.org/10.1016/j.orgel.2011.08.010>.
49. Sassi, M.; Crippa, M.; Ruffo, R.; Turrisi, R.; Drees, M.; Pandey, U. K.; Termine, R.; Golemme, A.; Facchetti, A.; Beverina, L. Open Circuit Voltage Tuning through Molecular Design in Hydrazone End Capped Donors for Bulk Heterojunction Solar Cells. *J. Mater. Chem. A* **2013**, *1* (7), 2631. <https://doi.org/10.1039/c2ta00673a>.
50. Shen, P.; Liu, X.; Jiang, S.; Wang, L.; Yi, L.; Ye, D.; Zhao, B.; Tan, S. Synthesis of New *N,N*-Diphenylhydrazone Dyes for Solar Cells: Effects of Thiophene-Derived π -Conjugated Bridge. *Dyes Pigments* **2012**, *92* (3), 1042–1051. <https://doi.org/10.1016/j.dyepig.2011.08.014>.
51. Gao, P.; Tsao, H. N.; Teuscher, J.; Grätzel, M. Organic dyes containing fused acenes as building blocks: Optical, electrochemical and photovoltaic properties. *Chin. Chem. Lett.* **2018**, *29* (2), 289–292. <https://doi.org/10.1016/j.ccllet.2017.09.056>.
52. Xu, M.; Zhang, M.; Pastore, M.; Li, R.; De Angelis, F.; Wang, P. Joint electrical, photophysical and computational studies on D- π -A dye sensitized solar cells: the impacts of dithiophene rigidification. *Chem. Sci.* **2012**, *3*, 976–983. <https://doi.org/10.1039/C2SC00973K>.
53. Marco, A. B.; Martínez de Baroja, N.; Franco, S.; Garín, J.; Orduna, J.; Villacampa, B.; Revuelto, A.; Andreu, R. Dithienopyrrole as a Rigid Alternative to the Bithiophene π Relay in Chromophores with Second-Order Nonlinear Optical Properties. *Chem. Asian J.* **2015**, *10*, 188–197. <https://doi.org/10.1002/asia.201402870>.

